Appl. Math. Mech. -Engl. Ed., **46**(2), 391–402 (2025)

APPLIED MATHEMATICS AND MECHANICS (ENGLISH EDITION)

https://doi.org/10.1007/s10483-025-3213-8

Applications of variable thermal features for the bioconvective flow of Jeffrey nanofluids due to stretching surface with mass suction effects: Cattaneo-Christov model*

S. U. KHAN[1], M. GARAYEV[2], ADNAN[3], K. RAMESH[4,5,6], M. EL MELIGY[7,8], D. ABDUVALIEVA[9], M. I. KHAN[10,†]

1. Department of Mathematics, Namal University, Mianwali 42250, Pakistan;
2. Department of Mathematics, College of Science, King Saud University, Riyadh 11421, Saudi Arabia;
3. Department of Mathematics, Mohi-ud-Din Islamic University, Nerian Sharif 12080, Pakistan;
4. Department of Pure and Applied Mathematics, School of Mathematical Sciences, Sunway University, Petaling Jaya 47500, Malaysia;
5. Department of Mathematics, Graphic Era (Deemed to be University), Dehradun, Uttarakhand 248002, India;
6. Department of Mathematics, School of Chemical Engineering and Physical Sciences, Lovely Professional University, Punjab 144411, India;
7. Jadara University Research Center, Jadara University, Irbid 21110, Jordan;
8. Applied Science Research Center, Applied Science Private University, Amman 11937, Jordan;
9. Department of Mathematics and Information Technologies, Tashkent State Pedagogical University, Tashkent 100070, Uzbekistan;
10. Department of Mechanics and Engineering Science, Peking University, Beijing 100871, China

(Received Aug. 25, 2024 / Revised Dec. 6, 2024)

Abstract The thermal nanofluids have garnered widespread attention for their use in multiple thermal systems, including heating processes, sustainable energy, and nuclear reactions. Research on nanofluids has revealed that the thermal efficiencies of such materials are adversely affected by various thermal features. The purpose of the current work is to demonstrate the thermal analysis of Jeffrey nanofluids with the suspension of

* Citation: KHAN, S. U., GARAYEV, M., ADNAN, RAMESH, K., EL MELIGY, M., ABDUVALIEVA, D., and KHAN, M. I. Applications of variable thermal features for the bioconvective flow of Jeffrey nanofluids due to stretching surface with mass suction effects: Cattaneo-Christov model. *Applied Mathematics and Mechanics* (*English Edition*), **46**(2), 391–402 (2025) https://doi.org/10.1007/s10483-025-3213-8

† Corresponding author, E-mail: 2106391391@pku.edu.cn

microorganisms in the presence of variable thermal sources. The variable effects of thermal conductivity, Brownian diffusivity, and motile density are utilized. The investigated model also reveals the contributions of radiation phenomena and chemical reactions. A porous, saturated, moving surface with a suction phenomenon promotes flow. The modeling of the problem is based on the implementation of the Cattaneo-Christov approach. The convective thermal constraints are used to promote the heat transfer features. A simplified form of the governing model is treated with the assistance of a shooting technique. The physical effects of different parameters for the problem are presented. The current problem justifies its applications in heat transfer, coating processes, heat exchangers, cooling systems in microelectronics, solar systems, chemical processes, etc.

Key words Jeffrey nanofluid, bioconvection effect, variable thermal consequence, chemical reaction, numerical simulation

Chinese Library Classification O357
2010 Mathematics Subject Classification 76A05, 74F25, 76Rxx, 49M30

Nomenclature

u, v,	velocity components;	ϑ^*,	chemotaxis constant;
x, y,	coordinate axes, m;	α_3,	variable motile diffusivity factor;
$\Lambda_{\rm e}$,	electrical conductivity;	Ω_2,	concentration relaxation coefficient;
ν,	kinematic viscosity, $\rm m^2/s$;	α_2,	variable mass diffusivity coefficient;
$T_{\rm f}$,	convective temperature, K;	$S_{\rm w}$,	surface motile density;
$C_{\rm w}$,	surface concentration, $\rm kg/m^3$;	$D_S(S)$,	variable motile diffusivity;
$\rho_{\rm f}$,	density, $\rm kg/m^3$;	S_∞,	motile density at free stream;
T_∞,	free stream temperature, K;	β,	Deborah number;
$D_{\rm B}$,	Brownian diffusion, $\rm m^2/s$;	Pe,	Peclet number;
C_∞,	ambient concentration, $\rm kg/m^3$;	ω_a,	thermal relaxation parameter;
T_∞,	ambient temperature, K;	H,	Hartmann number;
λ,	relaxation to retardation time ratio;	$\gamma_{\rm p}$,	porosity constant;
$D_{\rm T}$,	thermophoresis coefficient;	$k_{\rm r}$,	reaction constant;
λ_1,	retardation constant;	$R_{\rm d}$,	radiation parameter;
$k(T)$,	thermal conductivity;	Bi,	Biot number;
α_1,	variable thermal conductivity factor;	Pr,	Prandtl number;
k^*,	permeability of porous space;	$N_{\rm b}$,	Brownian constant;
Φ,	porous medium;	$N_{\rm t}$,	thermophoresis parameter;
τ,	ratio among heat capacities;	$\omega_{\rm b}$,	concentration relaxation parameter;
Λ^*,	maximum speed for swimming cell;	Sc,	Schmidt number;
$\kappa_{\rm c}$,	reactive species coefficient;	$L_{\rm b}$,	bioconvective Lewis number;
Ω_1,	thermal relaxation coefficient;	δ,	suction constant;
Ω,	absorption coefficient;	Nu,	Nusselt coefficient;
$\hbar$,	heat transfer;	Sh,	Sherwood coefficient;
κ_ϑ,	reaction coefficient;	$N_{\rm n}$,	motile density number.
Ξ,	Stefan Boltzmann constant;		

1 Introduction

Heat transfer is essential for various engineering processes and industrial systems. The vital role of heat transfer is exhibited in thermal processes, cooling systems, and the design of various electronic products. In energy systems, effective heat transfer is necessary to optimize the thermal efficiency of power systems, renewable energy devices, minimizing the energy cost and heating, ventilation, air conditioning (HVAC) system. Applications of heat transfer include heavy machinery, engine cooling, chemical reactors, and control systems. Various studies have aimed to describe heat transfer in different configurations. Wang et al.[1] observed the massive transport of heat transfer subject to vibration-induced systems. Wu et al.[2] conducted the

heat transfer analysis of rough surfaces subjected to horizontal vibrations. Huang et al.[3] addressed the vibro-convective turbulence phenomenon in microgravity applications. Wu et al.[4] investigated the heat transfer associated with thermal turbulence under the constraints of high Rayleigh numbers. Hsiao[5] evaluated the pivotal role of heat transfer in thermal extrusion systems under the flow of Maxwell fluids.

Leveraging their peak thermal outcomes and more stable heat fluctuation properties, researchers have continuously targeted different applications of nanofluids in diverse engineering and industrial fields. Recent advances in thermal engineering confirmed the applicability of nanofluids in different energy systems, chemical processes, thermal management recovery, cooling applications, solar energy, etc. A nanofluid represents a special decomposition between the base materials and metallic particles. The primary objective of this decomposition is to improve the thermal capacitance of base fluids. Nanofluids exhibit unique thermal mechanisms and properties, such as nanoparticle volume fraction, specific heat, buoyancy forces, and density. Nanofluids are highly promising for optimizing heat transfer and improving energy production. Recent studies indicated a wide range of research on this topic. Hsiao[6] addressed the significance of heat transfer in manufacturing processes with the application of Carreau nanofluids. Optimized results were proposed with the help of a parameter control approach. Hsiao[7] investigated nanofluids with slip boundary conditions. In another analysis, Hsiao[8] considered the role of viscous dissipation in micropolar nanofluid flow subject to novel multimedia features. Nazir et al.[9] studied nanofluid thermal interference owing to nanofluids in triangular cavity flow in the presence of a radiative framework. Bilal et al.[10] utilized the heat transfer visualization of the nanofluid flow by incorporating a modified transport model. Rahman et al.[11] investigated the thermal recruitment of iron oxide and titanium oxide nanoparticles for rotating disk flow. Zaheer et al.[12] proposed the buoyancy driven flow of nanofluids according to stagnation point analyses. Islam et al.[13] reported the vertically driven nanofluid flow with double diffusion prediction. Haider et al.[14] summarized observations of nanofluids for peristalsis flow subject to blood flow in the human body. Ramasekhar and Jawad[15] addressed the thermos-diffusion features of water-based nanofluids via a moving wedge. Carbon nanotubes (CNTs) and copper nanoparticles were used to analyze their thermal significance. Al Arni et al.[16] examined the transportation of nanofluids for oscillating flow caused by the interference of slip effects. Elboughdiri et al.[17] conducted an investigation of nanofluids in a chemically reactive flow associated with multi-sinusoidal passages. Li et al.[18] performed a communication to analyze heat transfer subject to the rotating disk flow of Maxwell nanofluids in porous media. Sahoo et al.[19] considered the Binary chemical reaction flow in an inclined channel containing nanomaterials. Mishra et al.[20] determined the role of different temperature constraints on nanofluid flow involving vibratory motion. Rezaee[21] reported the impact of nanofluids in order to describe the heat management of the Jeffrey Hamel flow. Mahitha et al.[22] visualized the upright flow of nanofluids using the fractional model.

The collective movement of self-organized microorganisms in nanofluids is described by bioconvection phenomena. Heat and mass transfer can be significantly influenced by bioconvection. Nanoparticles interact with microorganisms (bacteria and algae), which can swim upward. Such upward movement is associated with chemotaxis or phototaxis, leading to form a density gradient. The bioconvection phenomenon is preferred for improving the thermal stability of nanofluids. Bioconvection applications are realized in bio-reactors, enzymes, bio-heat systems, microbial fuel cells, etc. Waqas et al.[23] provided an insight into bioconvection while discussing the Jeffrey nanofluids in the presence of a magnetic dipole. Puneeth et al.[24] described the interactions of microorganisms in the Ree-Eyring nanofluid flow with the support of a theoretical model. Iqbal et al.[25] predicted the ionized flow of nanofluids by investigating the significant impact of bioconvection. Shamshuddin et al.[26] analyzed the bioconvective framework for the thermally depicted flow of nanofluids. Yu et al.[27] visualized the bioconvective prediction of jet flow driven by nanofluids. Abbas et al.[28] demonstrated the achievement of

stability via the suspension of microorganisms and nanofluids. Gasmi et al.[29] proposed the two-phase nanofluid flow with motile microorganisms. Jawad et al.[30] analyzed the detection of heat transfer using Casson nanofluids in the presence of microorganisms. Hussain et al.[31] developed a mathematical model for the micropolar nanofluid flow influenced by eukaryotic microbes. Rashed et al.[32] studied the permeable bioconvective flow in hybrid nanofluids using a numerical approach. Khan et al.[33] utilized the suction effects in the bioconvective flow of nanofluids with porous media.

This study conducts a bioconvective analysis of Jeffrey nanofluids subject to variable thermal properties, and investigates the porous saturated flow of Jeffrey nanofluids with mass suction effects. The analysis is performed under the consideration of variable thermal conductivity, Brownian diffusivity, and motile diffusivity. The key chemical reactions and thermal radiation features are elucidated. The upgraded model for the thermos-diffusion phenomenon (Cattaneo-Christov) is used to model the problem. A shooting scheme is used to complete the numerical task. A physical visualization of the results is presented for all the parameters involved.

2 Mathematical model

To elaborate the bioconvective aspects of Jeffrey nanofluids, a two-dimensional (2D) flow on a stretching surface with a porous medium is assumed. The suspension of microorganisms is considered to elaborate the bioconvection interpretation. The flow is laminar and incompressible. Suction effectiveness is also utilized. In the Cartesian frame, the velocity components are expressed with u and v along the surface and in the normal direction, respectively. The fluctuation in fluid movement is subject to the jerking of a flat plate with the velocity $u_{\mathrm{w}}(x) = ax$, where a is the stretching rate. The flow problem is illustrated in Fig. 1. The effects of the magnetic force are implemented with the magnetic force strength B_0. Variable effects are associated with the fluid thermal conductivity, motile density, and Brownian diffusivity. The radiated effects and chemical reaction features are included in the energy and concentration equations, respectively. The upgradation of the problem is subject to the implementation of the Cattaneo-Christov theory. The illustration of the problem is justified by the following modeled equations:

$$\frac{\partial u}{\partial x} + \frac{\partial v}{\partial y} = 0, \tag{1}$$

$$u\frac{\partial u}{\partial x} + v\frac{\partial u}{\partial y} = \frac{\nu}{1+\lambda}\Big(\frac{\partial^2 u}{\partial y^2} + \lambda_1\Big(v\frac{\partial^3 u}{\partial y^3} + u\frac{\partial^3 u}{\partial x \partial y^2} - \frac{\partial u}{\partial x}\frac{\partial^2 u}{\partial y^2} + \frac{\partial u}{\partial y}\frac{\partial^2 u}{\partial x \partial y}\Big)\Big) - \frac{\Lambda_{\mathrm{e}} B_0^2}{\rho_{\mathrm{f}}}u - \frac{\nu\Phi}{k^*}u, \tag{2}$$

$$u\frac{\partial T}{\partial x} + v\frac{\partial T}{\partial y} + \Omega_1\Big(u\frac{\partial v}{\partial x}\frac{\partial T}{\partial y} + u\frac{\partial u}{\partial x}\frac{\partial T}{\partial x} + u^2\frac{\partial^2 T}{\partial x^2} + v\frac{\partial v}{\partial y}\frac{\partial T}{\partial y} + v\frac{\partial u}{\partial y}\frac{\partial T}{\partial x} + v^2\frac{\partial^2 T}{\partial y^2} + 2uv\frac{\partial^2 T}{\partial x \partial y}\Big)$$
$$= \frac{16\Xi T_\infty^3}{3c_p\rho_{\mathrm{f}}\Omega}\frac{\partial^2 T}{\partial y^2} + \tau\Big(D_{\mathrm{B}}(C)\frac{\partial c}{\partial y}\frac{\partial T}{\partial y} + \frac{D_{\mathrm{T}}}{T_\infty}\Big(\frac{\partial T}{\partial y}\Big)^2\Big) + \frac{1}{c_p\rho_{\mathrm{f}}}\frac{\partial}{\partial y}\Big(k(T)\frac{\partial T}{\partial y}\Big), \tag{3}$$

$$u\frac{\partial C}{\partial x} + v\frac{\partial C}{\partial y} + \Omega_2\Big(2uv\frac{\partial^2 C}{\partial x \partial y} + u\frac{\partial u}{\partial x}\frac{\partial C}{\partial x} + u\frac{\partial v}{\partial x}\frac{\partial C}{\partial y} + v\frac{\partial v}{\partial y}\frac{\partial C}{\partial y} + u^2\frac{\partial^2 C}{\partial x^2} + v^2\frac{\partial^2 C}{\partial y^2} + v\frac{\partial u}{\partial y}\frac{\partial C}{\partial x}\Big)$$
$$= \frac{D_{\mathrm{T}}}{T_\infty}\frac{\partial^2 T}{\partial y^2} - \kappa_\vartheta(C - C_\infty) + \frac{\partial}{\partial y}\Big(D_{\mathrm{B}}(C)\frac{\partial C}{\partial y}\Big), \tag{4}$$

$$v\frac{\partial S}{\partial y} + u\frac{\partial S}{\partial x} + \frac{\vartheta^*\Lambda^*}{C_{\mathrm{w}} - C_\infty}\Big(\frac{\partial}{\partial y}\Big(S\frac{\partial C}{\partial y}\Big)\Big) = \frac{D_{\mathrm{T}}}{T_\infty}\frac{\partial^2 T}{\partial y^2}\frac{\partial}{\partial y}\Big(D_S(S)\frac{\partial S}{\partial y}\Big). \tag{5}$$

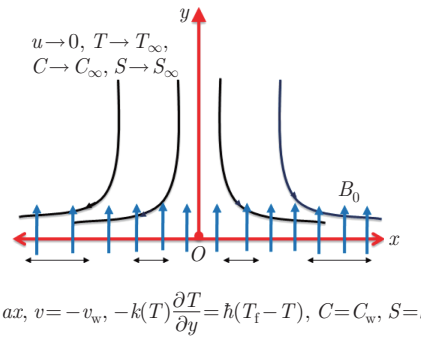

Fig. 1 Description of the flow problem (color online)

Define the variable relationships for $k(T)$, $D_{\mathrm{B}}(C)$, and $D_S(S)$ as follows:

$$k(T) = K_\infty\Big(1+\alpha_1\Big(\frac{T-T_\infty}{T_{\mathrm{f}}-T_\infty}\Big)\Big), \tag{6}$$

$$D_{\mathrm{B}}(C) = D_{B_0}\Big(1+\alpha_2\Big(\frac{C-C_\infty}{C_{\mathrm{w}}-C_\infty}\Big)\Big), \tag{7}$$

$$D_S(S) = D_{S_0}\Big(1+\alpha_3\Big(\frac{S-S_\infty}{S_{\mathrm{w}}-S_\infty}\Big)\Big). \tag{8}$$

The problem involves the following boundary conditions:

$$\begin{cases} u = u_{\mathrm{w}} = ax, \quad v = -v_{\mathrm{w}}, \quad -k(T)\dfrac{\partial T}{\partial y} = \hbar(T_{\mathrm{f}}-T), \quad C = C_{\mathrm{w}}, \quad S = S_{\mathrm{w}} \quad \text{at} \quad y = 0, \\ u \to 0, \quad T \to T_\infty, \quad C \to C_\infty, \quad S \to S_\infty \quad \text{as} \quad y \to \infty. \end{cases} \tag{9}$$

In the above equations, λ is the relaxation to retardation time ratio, D_{T} is the thermophoresis coefficient, C_{w} is the surface concentration, and λ_1 is the retardation constant. T_{f} is the convective temperature, Λ_{e} is the electrical conductivity, and ρ_{f} is the density. T_∞ is the free stream temperature, $k(T)$ is the thermal conductivity, and α_1 is the variable thermal conductivity factor. k^* denotes the permeability of the porous space, Φ represents the porous medium, and τ is the ratio of the heat capacities. D_{B} is the Brownian diffusion, Λ^* is the maximum speed for swimming cell, and C_∞ is the ambient concentration. κ_{c} is the reactive species coefficient, T_∞ is the ambient temperature, Ω_1 is the thermal relaxation coefficient, and Ω is the absorption coefficient. $\hbar$ is the heat transfer, κ_ϑ is the reaction coefficient, Ξ is the Stefan Boltzmann constant, and ϑ^* is the chemotaxis constant. Ω is the absorption coefficient, α_3 is the variable motile diffusivity factor, and Ω_2 is the concentration relaxation coefficient. α_2 is the variable mass diffusivity coefficient, S_{w} denotes the surface motile density, $D_S(S)$ is the variable motile diffusivity, and S_∞ is the free-stream motile density.

The problem can be simplified, with the interaction of the following new variables:

$$\begin{cases} v = -\sqrt{a\nu}f(\xi), \quad u = axf'(\xi), \quad \xi = \sqrt{\dfrac{a}{\nu}}y, \quad \theta(\xi) = \dfrac{T-T_\infty}{T_{\mathrm{f}}-T_\infty}, \\ \phi(\xi) = \dfrac{C-C_\infty}{C_{\mathrm{w}}-C_\infty}, \quad P(\xi) = \dfrac{S-S_\infty}{S_{\mathrm{w}}-S_\infty}. \end{cases} \tag{10}$$

The newly formulated system is as follows:

$$\begin{aligned} &f''' + \beta(f''^2 - ff'''') - (1+\lambda)(f'^2 - ff'') - (H+\gamma_{\mathrm{p}})(1+\lambda)f' = 0, \\ &(1+\alpha_1\theta + R_{\mathrm{d}})\theta'' + \alpha_1(\theta')^2 + Pr(f\theta' + N_{\mathrm{t}}\theta'^2) \\ &+ PrN_{\mathrm{b}}(1+\lambda_1\phi(\xi))\theta'\phi' - Pr\omega_a(f^2\theta'' + ff'\theta') = 0, \end{aligned} \tag{11}$$

$$(1+\alpha_2\phi)\phi'' - Sc\omega_b(ff'\phi' + f^2\phi'') + Scf\phi' - k_{\mathrm{r}}Sc\phi + \alpha_2\phi'^2 + \frac{N_{\mathrm{t}}}{N_{\mathrm{b}}}\theta'' = 0, \tag{12}$$

$$(1+\alpha_3 P)P'' + \alpha_3 P'^2 - Pe((P+\Gamma)\phi'' + P'\phi') + L_{\mathrm{b}}fP' = 0. \tag{13}$$

The simplified boundary conditions are

$$\begin{cases} f(0)=\delta, \quad f'(0)=0, \quad \theta'(0) = -Bi\Big(\dfrac{1-\theta(0)}{1+\lambda_1\theta(0)}\Big), \quad \phi(0)=0, \quad P(0)=1, \\ f'(\infty)\to 0, \quad \theta(\infty)\to 0, \quad \phi(\infty)\to 0, \quad P(\infty)\to 0, \end{cases} \tag{14}$$

where $\beta = \lambda_1 b$ (Deborah number), $Pe = \vartheta^*\Lambda^*/D_{\Gamma_0}$ (Peclet number), and $\omega_a = \Omega_a a$ (thermal relaxation parameter). $H = \Lambda_{\mathrm{e}}B_0^2/(\rho_{\mathrm{f}}b)$ (Hartmann number), $\gamma_{\mathrm{p}} = \nu\Phi/(k^*p)$ (porosity constant), and $k_{\mathrm{r}} = \kappa_\vartheta/a$ (reaction constant). $R_{\mathrm{d}} = 16\Xi T_\infty^3/(3k\Omega)$ (radiation parameter), $Bi = (\hbar/k)\sqrt{\nu/a}$ (Biot number), and $Pr = \mu c_p/k_\infty$ (Prandtl number). $N_{\mathrm{b}} = \tau D_{B_0}C_\infty/\nu$ (Brownian constant), and $N_{\mathrm{t}} = \tau D_{\mathrm{T}}(T_{\mathrm{f}}-T_\infty)/(T_\infty\nu)$ (thermophoresis parameter). $\omega_b = \Omega_b a$ (concentration relaxation parameter), $Sc = \nu/D_{\mathrm{B}}$ (Schmidt number), $L_{\mathrm{b}} = \nu_{\mathrm{f}}/D_{\Gamma_0}$ (bioconvective Lewis number), and $\delta = v_{\mathrm{w}}/\sqrt{\nu a}$ (suction constant).

The Nusselt coefficient, Sherwood coefficient, and motile density number are

$$\begin{cases} NuRe_x^{-0.5} = -(1+\alpha_1\theta'(0)+R_{\mathrm{d}})\theta'(0), \\ ShRe_x^{-0.5} = -(1+\alpha_2\phi(0))\phi'(0), \\ N_{\mathrm{n}}Re_x^{-0.5} = -(1+\alpha_3\chi(0))P'(0). \end{cases} \tag{15}$$

3 Numerical computations

Before analyzing the physical description of the problem, the formulated model is solved numerically. For computation, the shooting numerical scheme is used. The choice of the shooting scheme is based on favorable accuracy. To implement the numerical algorithm, a first-order system is developed with the following equations:

$$\begin{cases} f = G_1, \quad f' = G_2, \quad f'' = G_3, \quad f''' = G_4, \quad f'''' = G_4', \\ \theta = G_5, \quad \theta' = G_6, \quad \theta'' = G_6', \quad \phi = G_7, \quad \phi' = G_8, \quad \phi'' = G_8', \\ P = G_9, \quad P' = G_{10}, \quad P'' = G_{10}'. \end{cases} \tag{16}$$

The transformation of the problem becomes

$$G_4' = \frac{G_4 + \beta G_3^2 - (1+\lambda)(G_2^2 - G_1G_3) - (H+\gamma_{\mathrm{p}})(1+\lambda)G_2}{\beta G_1}, \tag{17}$$

$$\begin{aligned} G_6' = {} & \Big(\frac{1}{1+\alpha_1G_5+R_{\mathrm{d}}-Pr\omega_aG_1^2}\Big)(Pr\omega_a(G_1G_2G_6) - \alpha_1G_4^2 \\ & - PrN_{\mathrm{b}}(1+\alpha_1G_7)G_6G_8 - Pr(G_1G_6 + N_{\mathrm{t}}G_6^2)), \end{aligned} \tag{18}$$

$$G_8' = \Big(\frac{1}{1+\alpha_2G_7 - Sc\omega_bG_1^2}\Big)\Big(Sc\omega_bG_1G_2G_8 - \frac{N_{\mathrm{t}}}{N_{\mathrm{b}}}G_6' - ScG_1G_8 - \alpha_2G_8^2 + k_{\mathrm{r}}ScG_7\Big), \tag{19}$$

$$G_{10}' = \Big(\frac{1}{1+\alpha_3G_9}\Big)(Pe(G_8'(G_9+\delta) + G_{10}G_8) - L_{\mathrm{b}}G_1G_{10} - \lambda_3G_{10}^2) \tag{20}$$

with

$$G_1(0)=\delta, \quad G_2(0)=0, \quad G_6(0) = -Bi\Big(\frac{1-G_5(0)}{1+\lambda_1G_5(0)}\Big), \quad G_7(0)=1, \quad G_9(0)=1, \tag{21}$$

$$G_2(\infty)\to 0, \quad G_5(\infty)\to 0, \quad G_7(\infty)\to 0, \quad G_9(\infty)\to 0. \tag{22}$$

4 Validation of results

The validation of the numerical simulations is important for determining the solution accuracy. The results are validated under the limiting case in Table 1 based on the investigation by Turkyilmazoglu[34]. A favorable solution accuracy can be observed.

Table 1 Comparison of current results for $f''(0)$ when $\beta = \gamma_{\rm p} = 0$

H	Turkyilmazoglu[34]	Present result
0.5	−1.224 744 87	−1.224 744 89
1	−1.414 213 56	−1.414 213 57
1.5	−1.581 138 83	−1.581 138 83
2	−1.732 050 81	−1.732 050 84

5 Analysis of results

In this section, we predict the physical contributions of the involved parameters to investigate the velocity profile f', temperature profile θ, concentration field ϕ, and microorganisms profile P. Figure 2(a) shows the velocity profile f' under diverse variations in the Deborah number β. A reduction in f' is predicted with increasing β. The Deborah number is important in characterizing the rheology of non-Newtonian materials. The Deborah number is associated with fluid deformation, in which the particles take time to retain their original positions. Moreover, the Deborah number predicts the viscous, solid, and viscoelastic characteristics of non-Newtonian fluids. Figure 2(b) evaluates the significance of the retardation parameter λ. An increasing response of f' against upgraded values of λ is exhibited. The retardation fluid parameter denotes the fluid resistance in terms of deformation rate. Figure 2(c) shows the fluctuation of f' due to the suction parameter δ. Owing to suction, the velocity is reduced within the given domain. Such a decrement in f' is associated with the loss of fluids due to suction phenomena. The evaluation of f' by varying the porosity parameter $\gamma_{\rm p}$ is examined in Fig. 2(d). The executed response indicates a gradual decrease in f' with $\gamma_{\rm p}$. Physically, this decreasing variation is associated with the presence of permeability in the porous regime.

Figure 3(a) shows the impact of the variable thermal conductivity coefficient α_1 on the temperature profile θ. The temperature profile θ increases with an increase in α_1. Figure 3(b) shows the trend of θ with respect to the boosted effects of the retardation parameter. A slower variation is seen in the profile of θ for λ. Figure 3(c) displays θ upon increasing the suction parameter δ. The change in δ leads to increasing effects on θ. The results shown in Fig. 3(d) analyze the change in the profile of θ subject to larger values of the porosity parameter $\gamma_{\rm p}$. The porous media help increase the heat transfer. Such observations demonstrate key applications in petroleum engineering. Figure 3(e) shows the influence of thermal relaxation number ω_a on θ. A reduction is detected in θ for a peak range of ω_a. Figure 3(f) shows the important features of the thermophoresis parameter $N_{\rm t}$ on θ. As expected, increasing diversion is observed for θ owing to $N_{\rm t}$.

Figures 4(a)–4(e) show the physical visualizations of the concentration profile ϕ with increasing the Deborah number β, concentration relaxation parameter ω_b, variable Brownian diffusivity coefficient α_2, suction parameter δ, and chemical reaction constant $k_{\rm r}$. The changes in ϕ with various values of the Deborah number β are pronounced in Fig. 4(a). The increasing trend of ϕ due to β is displayed. Figure 4(b) shows the physical aspects of ϕ by incorporating the role of the concentration relaxation parameter ω_b. The concentration field is compressed due to ω_b. The variation in the variable Brownian diffusivity coefficient α_2 in the profile of ϕ is shown in Fig. 4(c). The consideration of the variable Brownian diffusivity leads to the enhancement of ϕ. Figure 4(d) displays the results of the concentration phenomenon to assess

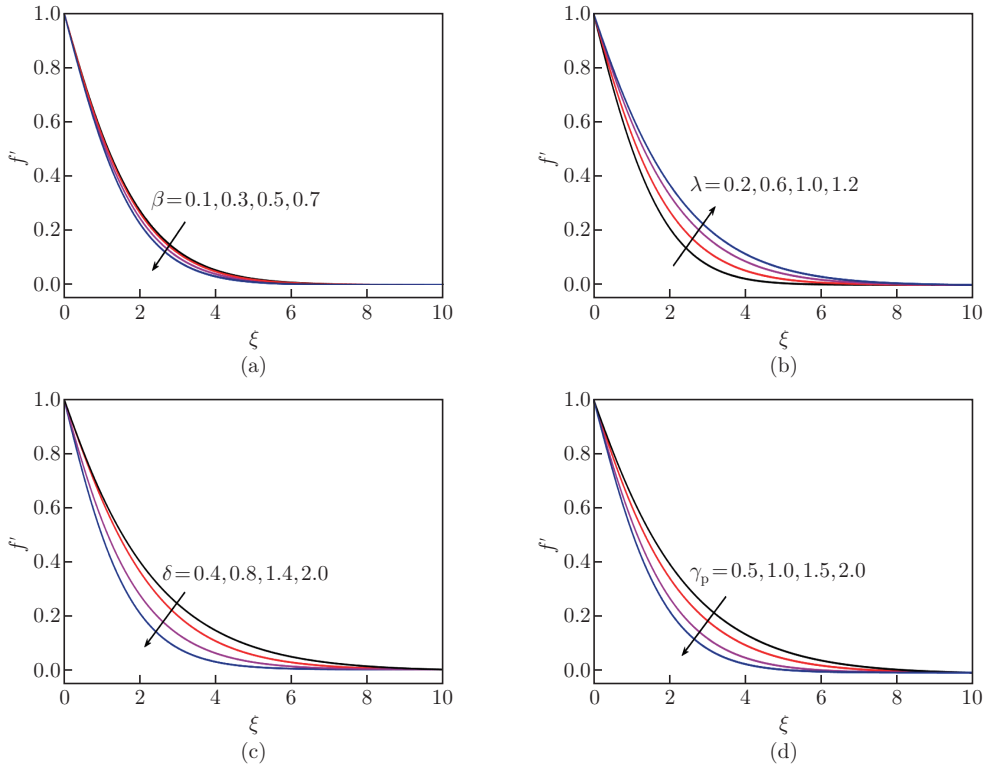

Fig. 2 Investigation of f' due to changes in (a) β, (b) λ, (c) δ, and (d) $\gamma_{\rm p}$ (color online)

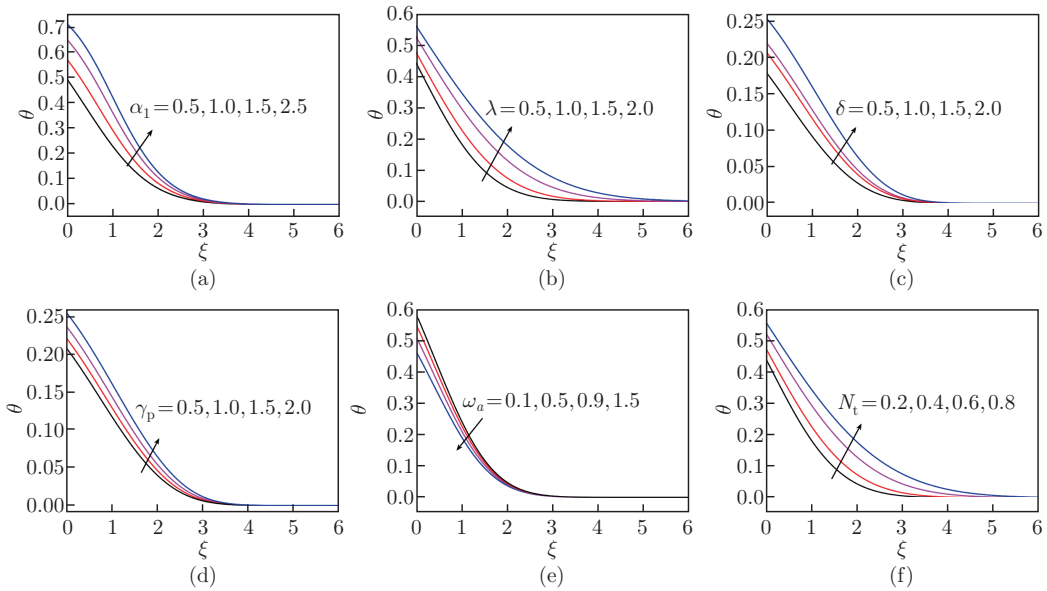

Fig. 3 Investigation of θ due to changes in (a) α_1, (b) λ, (c) δ, (d) $\gamma_{\rm p}$, (e) ω_a, and (f) $N_{\rm t}$ (color online)

the effects of the suction parameter δ. The concentration is enhanced for larger values of δ. Figure 4(e) shows the analysis of ϕ with increasing the chemical reaction parameter $k_{\rm r}$. With

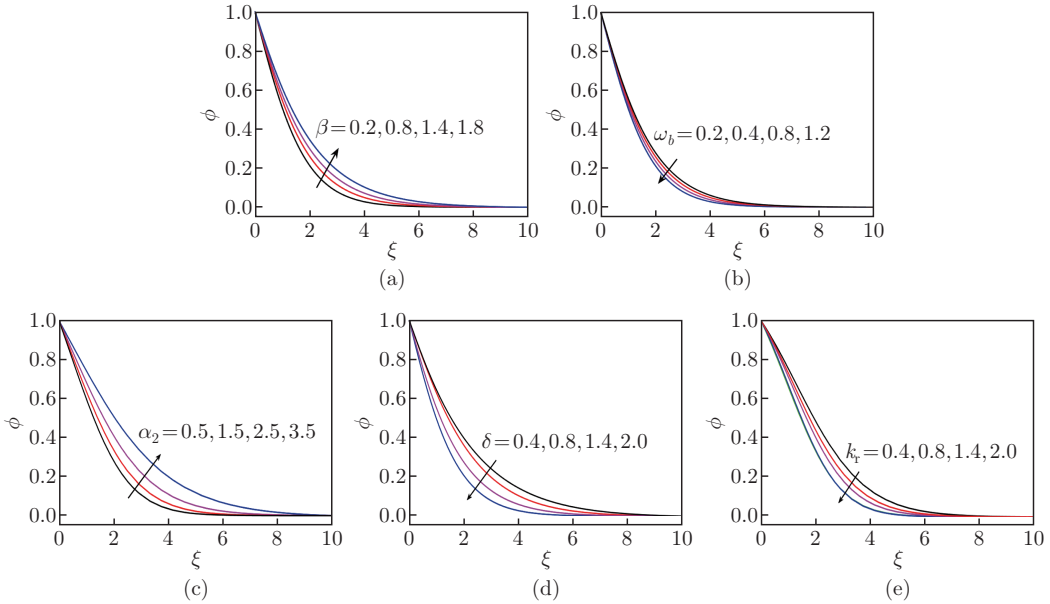

Fig. 4 Investigation of ϕ due to changes in (a) β, (b) ω_b, (c) α_2, (d) δ, and (e) k_r (color online)

effective values of k_r, a reduction in ϕ can be seen.

Figures 5(a)–5(c) show the insight inspired aspects of bioconvective phenomena by presenting the effects of various parameters on the microorganism profile P. The observations summarized in Fig. 5(a) comprise the role of Peclet number Pe on the microorganisms profile P. A declining role of Pe is reported for the microorganisms profile. Such outcomes are physically associated with a low motile diffusivity. Figure 5(b) shows that P gets improved with increasing the Deborah number β. The microorganism profile is enhanced for β. The influence of the variable motile diffusivity coefficient α_3 on P is shown in Fig. 5(c). By increasing α_3, the microorganism profile is boosted.

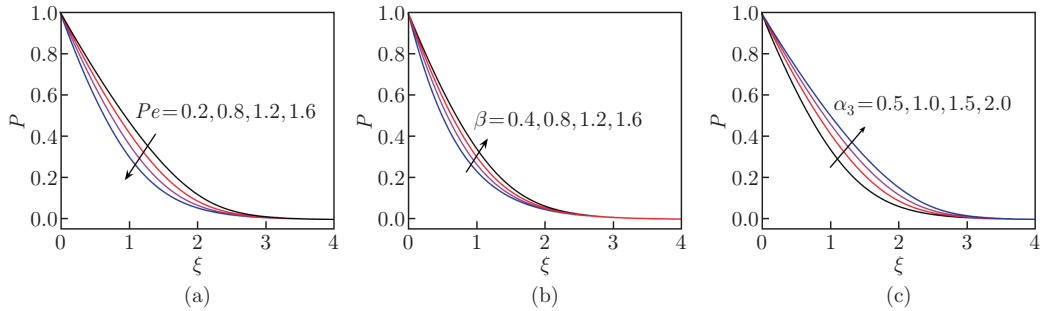

Fig. 5 Investigation of P due to changes in (a) Pe, (b) β, and (c) α_3 (color online)

Table 2 presents the numerical simulation results for the analyses of the Nusselt number, Sherwood number, and motile density number. The numerical results show that these quantities decrease with the porosity parameter γ_p, suction parameter δ, and Hartmann number H. Furthermore, the changes in the Prandtl number Pr and the retardation parameter λ lead to the improvement in these engineering quantities.

Table 2 Analysis for Nusselt number, Sherwood number, and motile density number

H	γ_{p}	δ	Pr	λ	Nusselt number	Sherwood number	Motile density number
0.2	0.1	0.3	0.3	0.5	0.827 41	0.662 44	0.556 43
0.4	0.1	0.3	0.3	0.5	0.776 23	0.650 64	0.533 13
0.6	0.1	0.3	0.3	0.5	0.728 54	0.632 33	0.526 45
0.6	0.4	0.3	0.3	0.5	0.789 51	0.625 43	0.590 53
0.6	0.8	0.3	0.3	0.5	0.777 53	0.575 36	0.574 67
0.6	1.4	0.3	0.3	0.5	0.752 68	0.530 54	0.567 85
0.6	1.4	0.2	0.3	0.5	0.838 90	0.645 34	0.544 50
0.6	1.4	0.6	0.3	0.5	0.810 15	0.626 75	0.523 38
0.6	1.4	1.0	0.3	0.5	0.789 37	0.597 51	0.487 42
0.6	1.4	1.0	0.2	0.5	0.885 32	0.572 33	0.569 85
0.6	1.4	1.0	0.4	0.5	0.935 32	0.588 87	0.597 69
0.6	1.4	1.0	0.6	0.5	0.993 34	0.616 87	0.619 51
0.6	1.4	1.0	0.6	0.4	0.809 73	0.694 47	0.607 53
0.6	1.4	1.0	0.6	1.0	0.775 32	0.716 87	0.622 48
0.6	1.4	1.0	0.6	1.6	0.740 37	0.737 41	0.653 21

6 Conclusions

The conclusions are drawn as follows.

(i) An upgraded velocity profile is observed owing to the variations in the retardation parameter.

(ii) The consideration of suction effects and saturated porous media leads to decreased velocities.

(iii) The temperature profile increases with increasing the variable thermal conductivity.

(iv) With dominant values of suction constant and thermophoresis parameter, larger heat transfer effects are observed.

(v) The temperature profile reduces with the thermal relaxation parameter.

(vi) The Deborah number and suction parameter have an increasing effect on the concentration profile.

(vii) The higher estimations of variable Brownian diffusivity lead to a decrease in the concentration profile.

(viii) The microorganism profile is enhanced when the variable motile diffusivity coefficient and the Deborah number increase.

Conflict of interest The authors declare no conflict of interest.

Data availability All data are available in the paper.

Acknowledgements The authors extend their appreciation to King Saud University for funding this work through researchers supporting project (No. RSPD2025R1056).

References

[1] WANG, B. F., ZHOU, Q., and SUN, C., Vibration-induced boundary-layer destabilization achieves massive heat-transport enhancement. *Science Advances*, **6**(21), eaaz8239 (2020)

[2] WU, J. Z., WANG, B. F., and ZHOU, Q. Massive heat transfer enhancement of Rayleigh-Bénard turbulence over rough surfaces and under horizontal vibration. *Acta Mechanica Sinica*, **38**(2), 321319 (2022)

[3] HUANG, Z. L., WU, J. Z., GUO, X. L., ZHAO, C. B., WANG, B. F., CHONG, K. L., and ZHOU, Q. Unifying constitutive law of vibroconvective turbulence in microgravity. *Journal of Fluid Mechanics*, **987**, A14 (2024)

[4] WU, J. Z., WANG, B. F., CHONG, K. L., DONG, Y. H., SUN, C., and ZHOU, Q. Vibration-induced 'anti-gravity' tames thermal turbulence at high Rayleigh numbers. *Journal of Fluid Mechanics*, **951**, A13 (2022)

[5] HSIAO, K. L. Combined electrical MHD heat transfer thermal extrusion system using Maxwell fluid with radiative and viscous dissipation effects. *Applied Thermal Engineering*, **112**, 1281–1288 (2017)

[6] HSIAO, K. L. To promote radiation electrical MHD activation energy thermal extrusion manufacturing system efficiency by using Carreau-nanofluid with parameters control method. *Energy*, **130**, 486–499 (2017)

[7] HSIAO, K. L. Stagnation electrical MHD nanofluid mixed convection with slip boundary on a stretching sheet. *Applied Thermal Engineering*, **98**, 850–861 (2016)

[8] HSIAO, K. L. Micropolar nanofluid flow with MHD and viscous dissipation effects towards a stretching sheet with multimedia feature. *International Journal of Heat and Mass Transfer*, **112**, 983–990 (2017)

[9] NAZIR, W., JAVED, T., ALI, N., and MUBBASHAR, N. Effects of radiative heat flux and heat generation on magnetohydodynamics natural convection flow of nanofluid inside a porous triangular cavity with thermal boundary conditions. *Numerical Methods for Partial Differential Equations*, **40**(2), e22768 (2024)

[10] BILAL, S., PAN, K., HUSSAIN, Z., KADA, B., PASHA, A. A., and KHAN, W. A. Darcy-Forchheimer chemically reactive bidirectional flow of nanofluid with magneto-bioconvection and Cattaneo-Christov properties. *Tribology International*, **193**, 109313 (2024)

[11] RAHMAN, M., TURKYILMAZOGLU, M., and MUSHTAQ, Z. Effects of multiple shapes for steady flow with transformer oil+Fe_3O_4+TiO_2 between two stretchable rotating disks. *Applied Mathematics and Mechanics* (*English Edition*), **45**(2), 373–388 (2024) https://doi.org/10.1007/s10483-024-3088-7

[12] ZAHEER, M., ABBAS, S. Z., HUANG, N., and ELMASRY, Y. Analysis of buoyancy features on magneto hydrodynamic stagnation point flow of nanofluid using homotopy analysis method. *International Journal of Heat and Mass Transfer*, **221**, 125045 (2024)

[13] ISLAM, A., MAHMOOD, Z., and KHAN, U. Significance of mixed convective double diffusive MHD stagnation point flow of nanofluid over a vertical surface with heat generation. *Proceedings of the Institution of Mechanical Engineers*, *Part N*: *Journal of Nanomaterials*, *Nanoengineering and Nanosystems* (2024) https://doi.org/10.1177/23977914231210798

[14] HAIDER, J. A., GUL, S., GEPREEL, K. A., KHAN, M. N., and LONE, S. A., Impact of heat transfer on peristaltic flow of nanofluid and its applications in real world problems. *Modern Physics Letters B*, **38**(6), 2350244 (2024)

[15] RAMASEKHAR, G. and JAWAD, M. Characteristics of MWCNT, SWCNT, Cu and water based on magnetized flow of nanofluid with Soret and Dufour effects induced by moving wedge: consequence of Falkner-Skan power law. *Numerical Heat Transfer*, *Part A*: *Applications* (2024) https://doi.org/10.1080/10407782.2024.2341270

[16] AL ARNI, S., EL JERY, A., ULLAH, Z., ALSULAMI, M. D., EL ZAHAR, E. R., SEDDEK, L. F., and BEN KHEDHER, N. Oscillatory and non-oscillatory analysis of heat and mass transfer of Darcian MHD flow of nanofluid along inclined radiating plate with Joule heating and multiple slip effects: microgravity analysis. *Case Studies in Thermal Engineering*, **60**, 104681 (2024)

[17] ELBOUGHDIRI, N., JAVID, K., SHEHZAD, M. Q., and BENGUERBA, Y. Influence of chemical reaction on electro-osmotic flow of nanofluid through convergent multi-sinusoidal passages. *Case Studies in Thermal Engineering*, **54**, 103955 (2024)

[18] LI, S., FAIZAN, M., ALI, F., RAMASEKHAR, G., MUHAMMAD, T., KHALIFA, H. A. E., and AHMAD, Z. Modelling and analysis of heat transfer in MHD stagnation point flow of Maxwell nanofluid over a porous rotating disk. *Alexandria Engineering Journal*, **91**, 237–248 (2024)

[19] SAHOO, R. K., MISHRA, S. R., and PANDA, S. Effective properties of binary chemical reaction with Brownian and thermophoresis on the radiative flow of nanofluid within an inclined heated channel. *Colloid and Polymer Science*, **302**, 1337–1352 (2024)

[20] MISHRA, S. K., TRIPURE, A., MISHRA, A., and SINGH, P. Effects of vibrational flow on nanofluid flow behavior under different temperature boundary conditions. *Numerical Heat Transfer*, *Part A*: *Applications* (2024) https://doi.org/10.1080/10407782.2024.2340071

[21] REZAEE, D. Linear temporal stability of Jeffery-Hamel flow of nanofluids. *European Journal of Mechanics-B/Fluids*, **107**, 1–16 (2024)

[22] MAHITHA, O., GOLLA, V. K. A., AKGÜL, A., and BANGALORE, R. K. New YAC time-fractional derivative approach for water-based hydromagnetic chemically reacting radiative flow of nanofluid with copper nanoparticles past an upright plate. *Numerical Heat Transfer*, *Part B*: *Fundamentals* (2024) https://doi.org/10.1080/10407790.2024.2345703

[23] WAQAS, H., HUSSAIN, M., ALQARNI, M. S., EID, M. R., and MUHAMMAD, T. Numerical simulation for magnetic dipole in bioconvection flow of Jeffrey nanofluid with swimming motile microorganisms. *Waves in Random and Complex Media*, **34**(3), 1958–1975 (2024)

[24] PUNEETH, V., ALI, F., KHAN, M. R., ANWAR, M. S., and AHAMMAD, N. A. Theoretical analysis of the thermal characteristics of Ree-Eyring nanofluid flowing past a stretching sheet due to bioconvection. *Biomass Conversion and Biorefinery*, **14**(7), 8649–8660 (2024)

[25] IQBAL, M., KHAN, N. S., KHAN, W., HASSINE, S. H., ALHABEEB, S. A., and KHALIFA, H. A. E. Partially ionized bioconvection Eyring-Powell nanofluid flow with gyrotactic microorganisms in thermal system. *Thermal Science and Engineering Progress*, **47**, 102283 (2024)

[26] SHAMSHUDDIN, M. D., SAEED, A., MISHRA, S. R., KATTA, R., and EID, M. R. Homotopic simulation of MHD bioconvective flow of water-based hybrid nanofluid over a thermal convective exponential stretching surface. *International Journal of Numerical Methods for Heat & Fluid Flow*, **34**(1), 31–53 (2024)

[27] YU, L. P., LI, Y. J., PUNEETH, V., SINGH, C., SINGHAL, A., and ANWAR, M. S. Thermal optimisation through the stratified bioconvective jetflow of nanofluid. *Numerical Heat Transfer*, *Part B*: *Fundamentals*, **85**(6), 791–804 (2024)

[28] ABBAS, M., KHAN, N., and SHEHZAD, S. A. Numerical analysis of Marangoni convected dusty second-grade nanofluid flow in a suspension of chemically reactive microorganisms. *Proceedings of the Institution of Mechanical Engineers*, *Part C*: *Journal of Mechanical Engineering Science*, **238**(10), 4400–4417 (2024)

[29] GASMI, H., OBALALU, A. M., AKINDELE, A. O., SALAUDEEN, S. A., KHAN, U., ISHAK, A., ABBAS, A., MUHAMMAD, T., HUSSAIN, S. M., and ABED, A. M. Thermal performance of a motile-microorganism within the two-phase nanofluid flow for the distinct non-Newtonian models on static and moving surfaces. *Case Studies in Thermal Engineering*, **58**, 104392 (2024)

[30] JAWAD, M., HUSSAIN, S., OUDINA, F. M., and SHEHZAD, K. Insinuation of radiative bioconvective MHD flow of Casson nanofluid with activation energy and swimming microorganisms. *Mathematical Modelling of Fluid Dynamics and Nanofluids*, 343–362 (2024)

[31] HUSSAIN, S. M., MAJEED, A., IJAZ, N., OMER, A. S. A., KHAN, I., MEDANI, M., and KHEDHER, N. B. Heat transfer in three dimensional micropolar based nanofluid with electromagnetic waves in the presence of eukaryotic microbes. *Alexandria Engineering Journal*, **94**, 339–353 (2024)

[32] RASHED, A. S., EHSAN, H. N., and MABROUK, S. M. Influence of gyrotactic microorganisms on bioconvection in electromagnetohydrodynamic hybrid nanofluid through a permeable sheet. *Computation*, **12**(1), 17 (2024)

[33] KHAN, M. I., AL KHALED, K., KHAN, S. U., IMTIAZ, M., and NORBERDIYEVA, M. Combined effects of nonlinear thermal radiation and suction/injection on bioconvective boundary layer of Maxwell nanofluid over a porous movable surface. *Numerical Heat Transfer*, *Part A*: *Applications* (2024) https://doi.org/10.1080/10407782.2024.2372039

[34] TURKYILMAZOGLU, M. The analytical solution of mixed convection heat transfer and fluid flow of a MHD viscoelastic fluid over a permeable stretching surface. *International Journal of Mechanical Sciences*, **77**, 263–268 (2013)